Korean J. Chem. Eng., **25**(6), 1389-1396 (2008)

Preparation, electrochemical properties, and cycle mechanism of $Li_{1-x}Fe_{0.8}Ni_{0.2}O_2$-$Li_xMnO_2$ (Mn/(Fe+Ni+Mn)=0.8) material

Gum-Jae Park*, Jung-Bae Heo*, Seung-Hyun Cho*, Sang-Ho Park, Hee-Sung Ahn***, and Yun-Sung Lee*,†**

*Faculty of Applied Chemical Engineering, Center for Functional Nano Fine Chemicals, Chonnam National University, 300 Yongbong-dong, Gwang-ju 550-757, Korea
**Energy Business Division Development Team, Samsung SDI Co. Ltd., 508 Sungsung-dong, Cheonan 330-300 Korea
***Korea Electrical Engineering & Science Research Institute, Seoul National University, San 56-1 Sillim-dong, Seoul 151-742, Korea
(*Received 20 February 2008 • accepted 7 May 2008*)

Abstract−A new type of $Li_{1-x}Fe_{0.8}Ni_{0.2}O_2$-$Li_xMnO_2$ (Mn/(Fe+Ni+Mn)=0.8) material was synthesized at 350 °C in an air atmosphere by a solid-state reaction. The material had an XRD pattern that closely resembled that of the original $Li_{1-x}FeO_2$-Li_xMnO_2 ((Fe+Ni+Mn)=0.8) with much reduced impurity peaks. It was composed of many large particles of about 500-600 nm and small particles of about 100-200 nm, which were distributed among the larger particles. The $Li/Li_{1-x}Fe_{0.8}Ni_{0.2}O_2$-$Li_xMnO_2$ cell showed a high initial discharge capacity above 192 mAh/g, which was higher than that of the parent $Li/Li_{1-x}FeO_2$-Li_xMnO_2 (186 mAh/g). This cell exhibited not only a typical voltage plateau in the 2.8 V region, but also an excellent cycle retention rate (96%) up to 45 cycles. We suggest a unique role of doped nickel ion in the $Li/Li_{1-x}Fe_{0.8}Ni_{0.2}O_2$-$Li_xMnO_2$ cell, which results in the increased initial discharge capacity from the redox reaction of Ni^{2+}/Ni^{3+} between 2.0 and 1.5 V region.

Key words: $Li_{1-x}FeO_2$-Li_xMnO_2, $Li_{1-x}Fe_{1-y}Ni_yO_2$-Li_xMnO_2, Role of Ni Ion, Lithium Secondary Battery

INTRODUCTION

The rapid development of electronics and communication industries has caused an enormous growth in portable devices such as cellular phones and laptop computers. This has led to an increasing demand for lightweight batteries with high energy density as power sources of portable devices. One of the various rechargeable batteries, the lithium secondary battery, has been considered as a promising power source of portable devices due to the higher volumetric and gravimetric energy densities compared to those of other rechargeable battery systems. The presently commercialized lithium secondary batteries use a layer structured $LiCoO_2$ cathode material. They had used a power source for small portable devices because they showed a stable charge/discharge profile and an excellent cycle performance. However, they had problems such as the high cost and toxicity of cobalt, which has become big problem for large scale batteries [1-3].

Today, new cathode materials are required for large scale battery operations that meet the dual requirements of cost and safety, in order to successfully commercialize hybrid electric vehicles (HEV) in lithium secondary batteries [4-6]. The Fe-based material is one of the best candidates from the viewpoint of cost and environment because iron is the most abundant and cheapest metal in the world. However, many problems still remain in $LiFeO_2$ such as a lower operating voltage which is caused by the fact that the $Fe^{4+/3+}$ redox energy in the $LiFeO_2$ structure tends to lie too far below the Fermi energy of the lithium anode and the $Fe^{3+/2+}$ couple is too close to it, no electrochemical activity, and a poor cycle characteristic during cycling test [7-15].

In an attempt to solve this problem, Lee et al. [16,17] developed a new type of the solid solution $Li_{1-x}FeO_2$-Li_xMnO_2 material. The $Li/Li_{1-x}FeO_2$-Li_xMnO_2 (Mn/(Fe+Mn)=0.5) system exhibited an excellent cycle characterization over 140 mAh/g until 50 cycles as well as a higher distinct voltage plateau (2.8 V) region against that of the $Li/Li_{1-x}FeO_2$ system [16]. Additionally, we believe it was quite noteworthy from the viewpoint of cost and environmental aspect because this system consisted of two main cheap transition metals (Fe and Mn).

However, we also realized that the $Li/Li_{1-x}FeO_2$-Li_xMnO_2 (Mn/(Fe+Mn)=0.5) cell showed a small initial discharge capacity (137 mAh/g) and the final capacity after a long-term cycling was still unsatisfactory as a practical lithium secondary battery [16,17]. What is needed is improved electrochemical properties of $Li/Li_{1-x}FeO_2$-Li_xMnO_2, and this work also could be very important for developing a new cathode material for large scale batteries.

In this paper, we report the synthesis, electrochemical properties, and cycle mechanism of a new type of $Li/Li_{1-x}Fe_{0.8}Ni_{0.2}O_2$-$Li_xMnO_2$ (Mn/(Fe+Ni+Mn)=0.8) cell using various analysis tools. Furthermore, we suggest a unique effect of doped nickel ions in the $Li/Li_{1-x}Fe_{0.8}Ni_{0.2}O_2$-$Li_xMnO_2$ cell, which can explain the reason why this cell showed the increased initial discharge capacity during charge/discharge process.

EXPERIMENTAL

$Li_{1-x}Fe_{0.8}Ni_{0.2}O_2$-$Li_xMnO_2$ material (Mn/(Fe+Ni+Mn)=0.8) was synthesized using $LiOH{\cdot}H_2O$ (Junsei Chemical, Japan), γ-FeOOH (High Purity Chemicals, Japan), $Ni(OH)_2$ (Junsei Chemical, Japan), and γ-MnOOH (Tosoh Chemical, Japan) by solid-state method. A

†To whom correspondence should be addressed.
E-mail: leeys@chonnam.ac.kr

stoichiometric amount of each material was ground and calcined at 300 ºC for 10 h and 350 ºC for 10 h in an air atmosphere using a box furnace. The Mn/(Fe+Ni+Mn) in this text means the molar ratio of metal ions used in synthesis is 0.8 without any explanation. The Li, Fe, Ni and Mn contents in the resulting material were analyzed by atomic absorption spectroscopy (AAS, AA-6200, Shimadzu, Japan) after dissolving the powder in dilute nitric acid. Powder X-ray diffraction (XRD, Rint 1000, Rigaku, Japan) using CuKα radiation was used to identify the crystalline phase of the synthesized material. Oxidation states of Fe, Ni, and Mn in the structure were investigated by x-ray photoelectron spectroscopy (XPS, VG Inc. MultiLab 2000, UK). Each sample was determined after drying at 120 ºC for 24 h. The source was monochromatic Al Kα radiation with a scan range of 1,100-0 eV of binding energy. The collected high-resolution XPS spectra were analyzed with an XPS peak software fitting program. The energy scale was adjusted on the carbon peak in C_{1s} spectra at 284.6 eV. The accuracy of the reported binding energy values was estimated to be ±0.2 eV. A transmission electron microscope (TEM, JEM 2010, JEOL, Japan) equipped with energy-dispersive x-ray spectrometer (EDS) was used to characterize the microstructure of powder. The electrochemical characterizations were performed with a CR2032 coin-type cell. The cathode was fabricated with 20 mg of accurately weighed active material and 12 mg of conductive binder (8 mg of Teflonized acetylene black (TAB) and 4 mg of graphite). It was pressed on 200 mm^2 stainless steel mesh used as the current collector under a pressure of 300 kg/cm^2 and dried at 130 ºC for 5 h in an oven. The test cell was made of a cathode and a lithium metal anode separated by a porous polypropylene film (Celgard 3401). The electrolyte used was a mixture of 1 M $LiPF_6$-ethylene carbonate (EC)/dimethyl carbonate (DMC) (1 : 2 by Vol., Ube Chemicals, Japan). The charge and discharge current density was 0.4 mA/cm^2 with a cut-off voltage of 1.5 to 4.5 V at room temperature. A three-electrode glass cell was used for cyclic voltammetry measurement. The working electrode consisted of 3 mg of the active material and 2.2 mg of conducting binder (TAB), which was pressed onto stainless steel mesh. The counter and reference electrodes were prepared by pressing lithium foil onto stainless steel gauze. The CV measurement was performed with a Hokuto Denko system (HSV-100, Japan) at 0.2 mV/s scan rate between the voltage limits of 1.5-4.5 V. All of the cell was assembled in a dry box with argon gas.

RESULTS AND DISCUSSION

In order to prevent cation mixing (or disordering) of each transition metal ion in the structure during the synthetic process, a transition metal was substituted into $Li_{1-x}FeO_2$-Li_xMnO_2 material by two kinds of synthetic methods. The optimum doping metal and the sites which can be easily substituted by metal ions in the structure, still need to be investigated and determined because $Li_{1-x}FeO_2$-Li_xMnO_2 material has two kinds of cations (Fe=0.69 Å) and (Mn=0.72 Å). In order to try successful substitution of metal ions with similar ionic radius, the substitution of nickel (0.69 Å) into the $Li_{1-x}FeO_2$-Li_xMnO_2 material was conducted as follows. One is the synthesis of $Li_{1-x}FeO_2$ at 300 ºC in advance and the addition of the $Mn_{0.8}Ni_{0.2}O_2$ (intermediate compound) before calcination at 350 ºC. The other is the preparation of $Li_{1-x}Fe_{0.8}Ni_{0.2}O_2$ (intermediate compound) material beforehand and addition of Mn source before calcination at 350 ºC. In the former method, the nickel ions are substituted into the manganese sites ($Li_{1-x}FeO_2$-$Li_xMn_{0.8}Ni_{0.2}O_2$), while in the latter, the nickel ions are substituted into the iron sites ($Li_{1-x}Fe_{0.8}Ni_{0.2}O_2$-$Li_xMnO_2$) of the $Li_{1-x}FeO_2$- Li_xMnO_2 system.

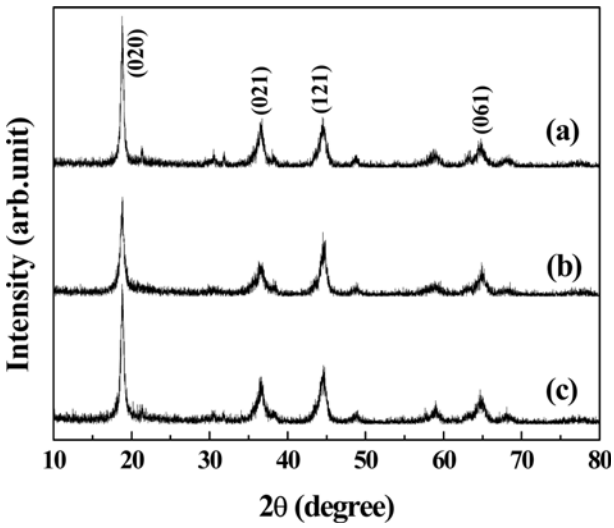

Fig. 1. X-ray diffraction patterns of (a) $Li_{1-x}FeO_2$-Li_xMnO_2 (Mn/(Fe+Ni+Mn)=0.8), (b) $Li_{1-x}FeO_2$-$Li_xMn_{0.8}Ni_{0.2}O_2$ (Mn/(Fe+Ni+Mn)=0.8), and (c) $Li_{1-x}Fe_{0.8}Ni_{0.2}O_2$-$Li_xMnO_2$ (Mn/(Fe+Ni+Mn)=0.8). These materials were calcined at 350 ºC for 10 h in air.

Fig. 1 shows XRD patterns of the original $Li_{1-x}FeO_2$-Li_xMnO_2, $Li_{1-x}FeO_2$-$Li_xMn_{0.8}Ni_{0.2}O_2$, and $Li_{1-x}Fe_{0.8}Ni_{0.2}O_2$-$Li_xMnO_2$ materials which were calcined at 350 ºC for 10 h in an air atmosphere. The original $Li_{1-x}FeO_2$-Li_xMnO_2 material exhibited an XRD pattern resembling that of the orthorhombic Li_xMnO_2 (Pnam) material [6]. The main peaks, (020) and (021), of the $Li_{1-x}FeO_2$-Li_xMnO_2 material were quite well developed, although peaks corresponding to a couple of impurities were observed in the range between 20 and 35º. $Li_{1-x}FeO_2$-$Li_xMn_{0.8}Ni_{0.2}O_2$ exhibited a similar XRD pattern compared to that of the $Li_{1-x}FeO_2$-Li_xMnO_2 material, as shown in Fig. 1(b). However, some of impurity peaks in the region between 20 and 35º almost disappeared in the case of this material and the intensities of (020) and (021) main peaks were slightly decreased compared with those of the original compound.

On the other hand, the $Li_{1-x}Fe_{0.8}Ni_{0.2}O_2$-$Li_xMnO_2$ material showed a different XRD pattern from that of the $Li_{1-x}FeO_2$-$Li_xMn_{0.8}Ni_{0.2}O_2$ material. The FWHMs of the main peaks of $Li_{1-x}Fe_{0.8}Ni_{0.2}O_2$-$Li_xMnO_2$ were decreased to the level of that of the original compound and the impurity peaks between 20 and 35º region, which were much diminished compared to those of the original material, still remained. In addition, it was found that some extra impurity peaks at 37º and 64º disappeared clearly in the XRD diagram. This means that the two types of nickel doped materials, $Li_{1-x}FeO_2$-$Li_xMn_{0.8}Ni_{0.2}O_2$ and $Li_{1-x}Fe_{0.8}Ni_{0.2}O_2$-$Li_xMnO_2$, were successfully substituted and stabilized into the $Li_{1-x}FeO_2$-Li_xMnO_2 structure by nickel ions. This indicates that nickel substitution in this study improved the crystallographic characterization of original $Li_{1-x}FeO_2$-Li_xMnO_2 material and might result in the enhancement of the electrochemical properties during the charge/discharge process.

Table 1. The results of XPS analysis for $Li_{1-x}FeO_2$-Li_xMnO_2 and nickel substituted $Li_{1-x}FeO_2$-Li_xMnO_2 (Mn/Fe+Ni+Mn=80%) materials

	$Li_{1-x}FeO_2$-Li_xMnO_2	$Li_{1-x}FeO_2$-$Li_xMn_{0.8}Ni_{0.2}O_2$	$Li_{1-x}Fe_{0.8}Ni_{0.2}O_2$-$Li_xMnO_2$
Fe	+3	+3	3+
Ni		+2, +3	+2
Mn	+4	+3, +4	+4

The best way to determine crystallographic properties of the prepared material is to conduct a Rietveld analysis. However, x-ray photoelectron spectroscopy (XPS) can also be one useful method for analyzing the state of original and substituted metal ions in the structure in conjunction with crystallographic analysis. In order to investigate the oxidation states of the Fe, Ni, and Mn ions, an XPS analysis was conducted on the $Li_{1-x}FeO_2$-Li_xMnO_2, $Li_{1-x}FeO_2$-$Li_xMn_{0.8}Ni_{0.2}O_2$, and $Li_{1-x}Fe_{0.8}Ni_{0.2}O_2$-$Li_xMnO_2$ materials, respectively. Each sample was determined after drying at 120 °C for 24 h in the vacuum oven. The high-resolution XPS spectra were analyzed by an XPS peak software fitting program. Table 1 shows the XPS results of various metal ions for the three materials. It was found that the ion state of Fe in the structure for all of materials is commonly 3+, with the spectra exhibiting complex profiles with a major component centered at 710.9 eV. However, the Mn and Ni ions exhibited quite different behaviors. The valence states of Mn ion of the $Li_{1-x}FeO_2$-Li_xMnO_2 and $Li_{1-x}Fe_{0.8}Ni_{0.2}O_2$-$Li_xMnO_2$ materials were both 4+, and the BE values for Mn $2p_{3/2}$ peaks of these two materials were 642.3 and 642.6 eV, respectively. However, the binding energy of the $Li_{1-x}FeO_2$-$Li_xMn_{0.8}Ni_{0.2}O_2$ material was 642.3 eV, which is slightly lower than that of $Li_{1-x}Fe_{0.8}Ni_{0.2}O_2$-$Li_xMnO_2$, which can be attributed to the presence of Mn ion in both the 3+ and 4+ valence states. Furthermore, the ion state of nickel in the $Li_{1-x}FeO_2$-$Li_xMn_{0.8}Ni_{0.2}O_2$ material was a mixture of 2+ (Ni $2p_{3/2}$=854.9 eV) and 3+ (Ni $2p_{3/2}$=856.7 eV), whereas that in $Li_{1-x}Fe_{0.8}Ni_{0.2}O_2$-$Li_xMnO_2$ was only 2+ (Ni $2p_{3/2}$=855.0 eV). Based on the above results, it could be expected that $Li_{1-x}Fe_{0.8}Ni_{0.2}O_2$-$Li_xMnO_2$ material presents very similar powder and electrochemical properties to those of the original material, because the Fe and Mn ions are in the same valence state and successful nickel substitution was observed by XPS analysis. Conversely, the $Li_{1-x}FeO_2$-$Li_xMn_{0.8}Ni_{0.2}O_2$ material might be expected to show poor electrochemical properties, owing to the existence of Mn and Ni ions in the various valence states in the structure, although it exhibited a very clear XRD pattern as shown in

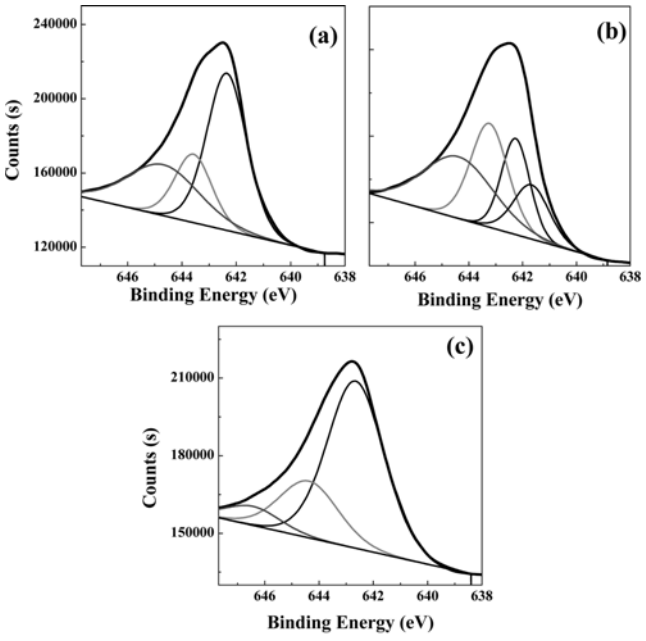

Fig. 2. XPS spectra of Mn $2p_{3/2}$ of (a) $Li_{1-x}FeO_2$-Li_xMnO_2 (Mn/(Fe+Ni+Mn)=0.8), (b) $Li_{1-x}FeO_2$-$Li_xMn_{0.8}Ni_{0.2}O_2$ (Mn/(Fe+Ni+Mn)=0.8), and (c) $Li_{1-x}Fe_{0.8}Ni_{0.2}O_2$-$Li_xMnO_2$ (Mn/(Fe+Ni+Mn)=0.8) materials.

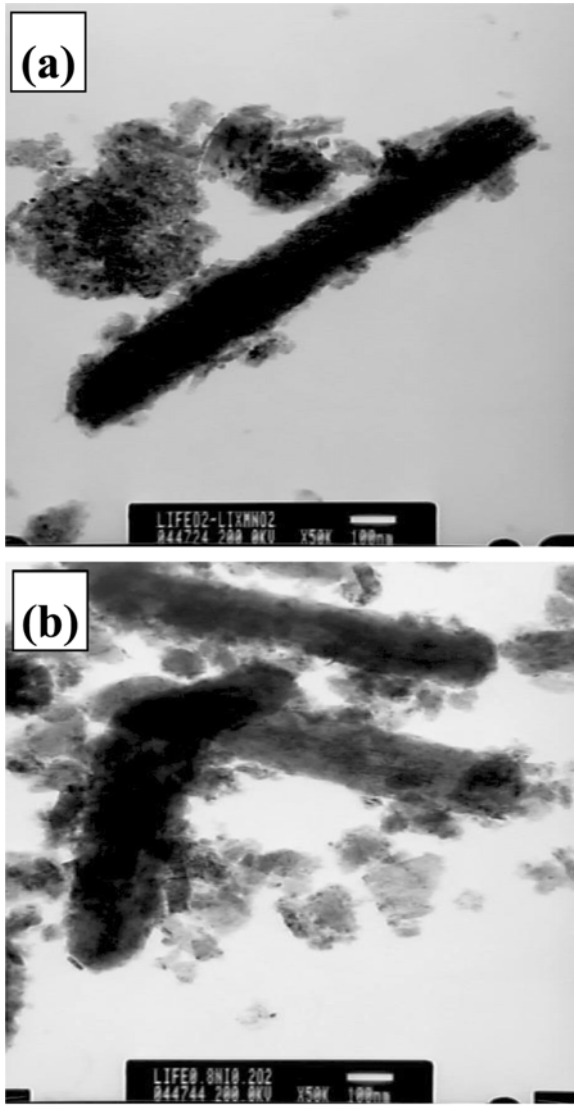

Fig. 3. TEM images of resulting materials. (a) bright field image of $Li_{1-x}FeO_2$-Li_xMnO_2 (Mn/(Fe+Ni+Mn)=0.8) and (b) $Li_{1-x}Fe_{0.8}Ni_{0.2}O_2$-$Li_xMnO_2$ (Mn/(Fe+Ni+Mn)=0.8) materials.

Fig. 1. We already confirmed this assumption using electrochemical analysis and cycling test as presented in a previous study. It also presented the XPS result of the Mn $2p_{3/2}$ spectra of the three materials as shown in Fig. 2, which confirms the difference of the Mn ion state between the $Li_{1-x}FeO_2$-$Li_xMn_{0.8}Ni_{0.2}O_2$ and $Li_{1-x}Fe_{0.8}Ni_{0.2}O_2$-$Li_xMnO_2$ materials. Furthermore, the Li/$Li_{1-x}FeO_2$-$Li_xMn_{0.8}Ni_{0.2}O_2$ cell, although the figure is not shown in this text, presents a diminished voltage plateau at 2.8 V, a reduced initial discharge capacity, and unstable charge/discharge profiles compared with the original Li/$Li_{1-x}FeO_2$-Li_xMnO_2 cell. The difference of the discharge capacity of Li/$Li_{1-x}FeO_2$-$Li_{1-x}Mn_{0.8}Ni_{0.2}O_2$ and Li/$Li_{1-x}Fe_{0.8}Ni_{0.2}O_2$-$Li_xMnO_2$ cells was 19 mAh/g, which represents a considerable total discharge capacity. Based on the above results, we suggest that the doped nickel ions are substituted not into the Mn sites, but into the Fe sites in the $Li_{1-x}FeO_2$-Li_xMnO_2 material, which is a very important consideration in the synthesis of Ni substituted $Li_{1-x}FeO_2$-Li_xMnO_2 materials.

Fig. 3 shows the transmission electron microscopy (TEM) images of $Li_{1-x}FeO_2$-Li_xMnO_2 and $Li_{1-x}Fe_{0.8}Ni_{0.2}O_2$-$Li_xMnO_2$ materials. Two materials have a similar particle shape and a particle size. We can confirm there is no big difference between the two materials in the particle distribution. The $Li_{1-x}FeO_2$-Li_xMnO_2 powder consisted of 500-600 nm with needle-type particles, which was shown to the compound using γ-MnOOH [19,20] or γ-FeOOH [18] as a starting material. Some other small particles at about 100-200 nm were distributed among the larger particles. A small part of needle-like large particles were located randomly and many small particles at about 100 nm were distributed among the larger particles.

Fig. 4 shows the initial charge/discharge curves of the Li/$Li_{1-x}FeO_2$-Li_xMnO_2 and the Li/$Li_{1-x}Fe_{0.8}Ni_{0.2}O_2$-$Li_xMnO_2$ cells. The test condition was a current density of 0.4 mA/cm^2 between 4.5 and 1.5 V. The first discharge curve of the Li/$Li_{1-x}FeO_2$-Li_xMnO_2 cell shows a high initial capacity over 186 mAh/g and also a distinct voltage plateau at 2.8 V in the discharge curve. We already reported that the existence of the voltage plateau at 2.8 V might result from the redox reaction from Mn^{4+} to Mn^{3+} in the Li_xMnO_2 compound [17]. This cell also showed two small voltage plateaus at about 2.0 V and 1.6 V, respectively, which are expected as an evidence of structural change during cycling. The initial discharge behavior of Li/$Li_{1-x}Fe_{0.8}Ni_{0.2}O_2$-$Li_xMnO_2$ cell is also shown in Fig. 4(b). It is interesting to find the difference in the discharge capacities between 2.8 to 4.5 V (herein referred to as $C_{2.8\text{-}4.5V}$) in the discharge curves of the two systems. The $C_{2.8\text{-}4.5V}$ values were 37 mAh/g and 57 mAh/g for the Li/$Li_{1-x}FeO_2$-Li_xMnO_2 cell and the Li/$Li_{1-x}Fe_{0.8}Ni_{0.2}O_2$-$Li_xMnO_2$ cell, respectively. The difference of $C_{2.8\text{-}4.5V}$ between the two cells was quite large and up to 20 mAh/g, which is a considerable total discharge capacity. The Li/$Li_{1-x}Fe_{0.8}Ni_{0.2}O_2$-$Li_xMnO_2$ cell exhibited a very high initial discharge capacity of 192 mAh/g, even though all increased capacity of $C_{2.8\text{-}4.5V}$ did not reflect. It might be assumed that nickel ions played an effective role to increase the initial discharge capacity of $Li_{1-x}Fe_{1.8}Ni_{0.2}O_2$-$Li_xMnO_2$ system.

Fig. 5 shows the variation in the specific discharge capacity with the number of cycles for the Li/$Li_{1-x}FeO_2$-Li_xMnO_2 and the Li/$Li_{1-x}Fe_{0.8}Ni_{0.2}O_2$-$Li_xMnO_2$ systems. The current density was 0.4 mA/cm^2 between 4.5 and 1.5 V. As reported before [17], the Li/$Li_{1-x}FeO_2$-Li_xMnO_2 (Mn/(Fe+Mn)=0.5) cell exhibited a small initial discharge capacity of 137 mAh/g and slightly increased capacity (158 mAh/g) until the 50th cycle, though it should be noted that this discharge capacity still falls short of that required for a practical battery system with high discharge capacity. However, the Li/$Li_{1-x}FeO_2$-Li_xMnO_2 (Mn/(Fe+Ni+Mn)=0.8) cell presented a high discharge capacity of 186 mAh/g and presented very high cycle retention rate of 96.1% after the 45th cycle. The Li/$Li_{1-x}Fe_{0.8}Ni_{0.2}O_2$-$Li_xMnO_2$ cell exhibited not only a very high initial discharge capacity of 192 mAh/g, but also an excellent cycle retention rate of 95.8% after 45 cycles. The higher initial discharge capacity of Li/$Li_{1-x}Fe_{0.8}Ni_{0.2}O_2$-$Li_xMnO_2$ cell

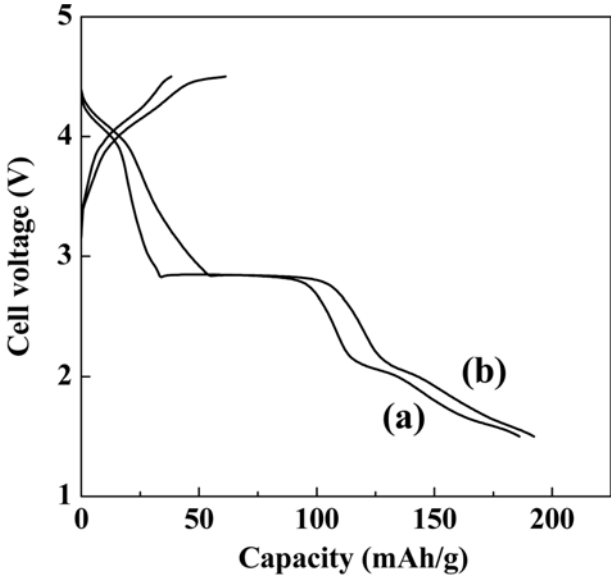

Fig. 4. The initial charge/discharge curves of the (a) Li/$Li_{1-x}FeO_2$-Li_xMnO_2 (Mn/(Fe+Ni+Mn)=0.8) and (b) Li/$Li_{1-x}Fe_{0.8}Ni_{0.2}O_2$-$Li_xMnO_2$ (Mn/(Fe+Ni+Mn)=0.8) cells. The test conditions were a current density of 0.4 mA/cm^2 between 1.5 and 4.5 V at room temperature.

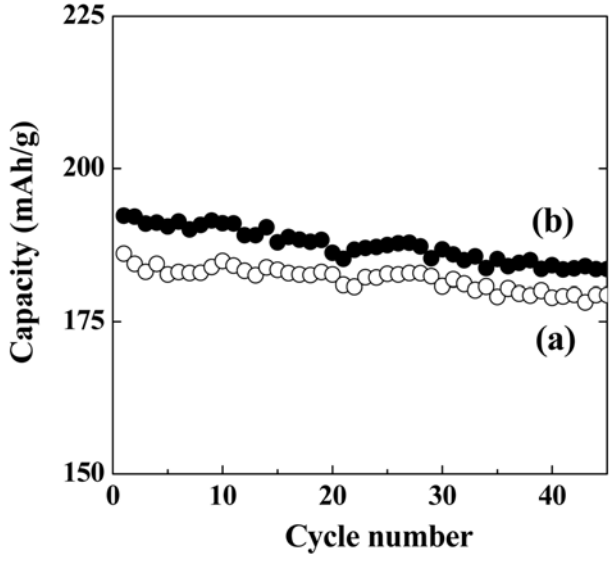

Fig. 5. Specific discharge capacity *vs.* cycle number for (a) Li/$Li_{1-x}FeO_2$-Li_xMnO_2 (Fe+Ni+Mn)=0.8) and (b) Li/$Li_{1-x}Fe_{0.8}Ni_{0.2}O_2$-$Li_xMnO_2$ (Mn/(Fe+Ni+Mn)=0.8) cells. The test conditions were a current density of 0.4 mA/cm^2 between 1.5 and 4.5 V at room temperature.

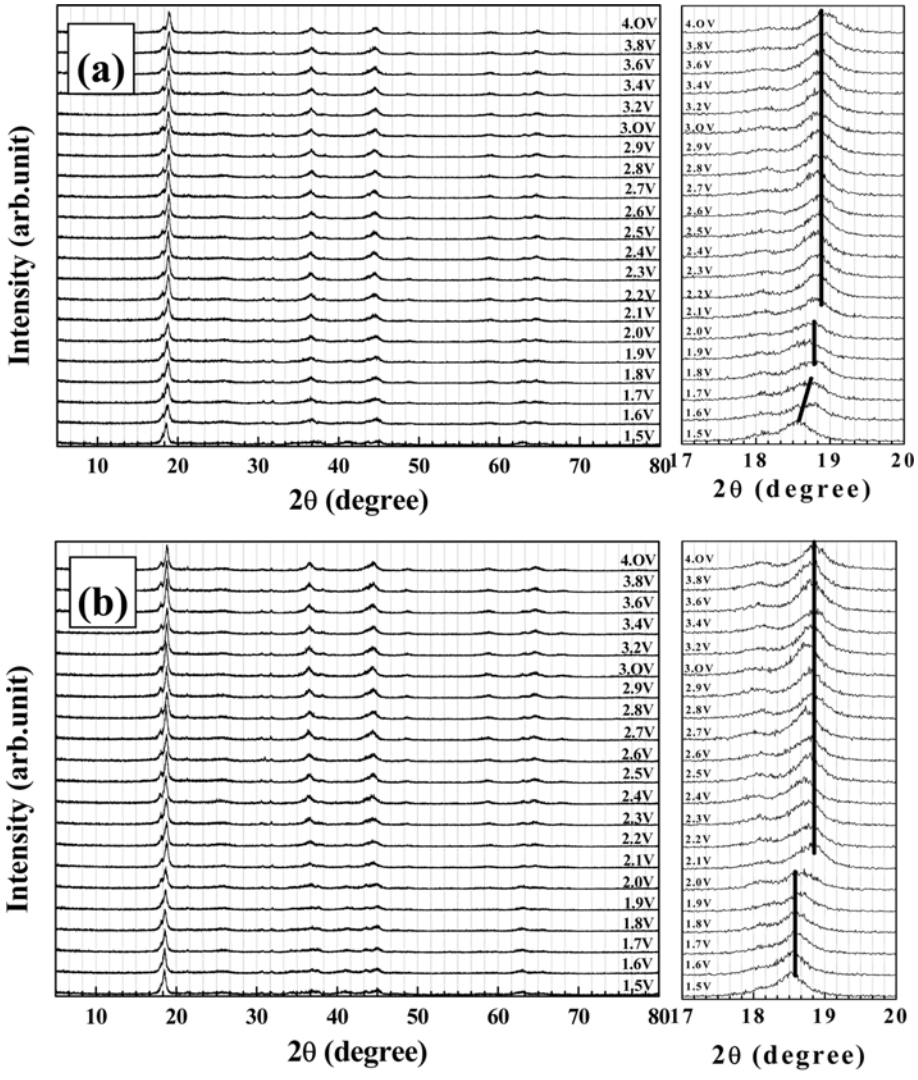

Fig. 6. *Ex-situ* XRD patterns of $Li/Li_{1-x}FeO_2$-Li_xMnO_2 (Mn/(Fe+Ni+Mn)=0.8) and (b) $Li/Li_{1-x}Fe_{0.8}Ni_{0.2}O_2$-$Li_xMnO_2$ (Mn/(Fe+Ni+Mn)=0.8) cells. The test conditions were a current density of 0.1 mA/cm^2 between 1.5 and 4.5 V at room temperature.

compared with the original system still remained after the long-term cycle test, although the difference in the discharge capacity between two cells gradually decreased with increasing number of cycles.

What is the main reason to induce a high discharge capacity of $Li/Li_{1-x}Fe_{0.8}Ni_{0.2}O_2$-$Li_xMnO_2$ cell in the cycle test? In a series of experiments, it could be expected that the doped nickel ion in the structure plays an important role in changing particle property, which can induce the alternation of electrochemical properties during the charge/discharge process. In order to investigate the structural changes of the two cells during cycling, *ex-situ* XRD measurements were taken of two $Li/Li_{1-x}FeO_2$-Li_xMnO_2 and $Li/Li_{1-x}Fe_{0.8}Ni_{0.2}O_2$-$Li_xMnO_2$ electrodes in the discharged state after the first cycle. Each cell was left in a glove box for 2 days to reach equilibrium after being tested from 1.5 V to 4.5 V.

Fig. 6(a) shows the *ex-situ* XRD pattern of $Li/Li_{1-x}FeO_2$-Li_xMnO_2 cell and also indicates the main peak of (020) from 17° to 20° for the comparison. All peaks in this XRD pattern show no big change during cycling. However, a small change of (020) main peak in the lower voltage region could be easily found, especially from 2.0 V to 1.5 V. The main (020) peak was maintained at the same position at 18.8° until 2.1 V and it slowly shifted to lower angle to 18.6° at 2.0 V in the XRD diagram. This indication maintained until 1.7 V and rapidly shifted to a much lower angle until 1.5 V. It means that $Li/Li_{1-x}FeO_2$-Li_xMnO_2 cell has two times of structural changes during the discharge process, which is well matched with two small voltage plateaus at about 2.0 V and 1.6 V in the discharge curve, as shown in Fig. 4(a). The $Li/Li_{1-x}Fe_{0.8}Ni_{0.2}O_2$-$Li_xMnO_2$ cell also shows very similar XRD pattern as like the $Li/Li_{1-x}FeO_2$-Li_xMnO_2 cell. The main peak was sustained at the same position until 2.1 V and other peaks also presented no remarkable peak shift in the whole XRD region. However, one difference is that there is no structural change between the 2.0 to 1.5 V region. It means that the $Li/Li_{1-x}Fe_{0.8}Ni_{0.2}O_2$-$Li_xMnO_2$ cell did not suffer from remarkable structural change, which the structure could maintain its original structure during cycling. This phenomenon also could be found and well matched in the charge/discharge curve of $Li/Li_{1-x}Fe_{0.8}Ni_{0.2}O_2$-$Li_xMnO_2$, as shown in Fig. 4(b). From the *ex*-situ XRD result, we could conclude that the peak shift of the two systems in the XRD pattern com-

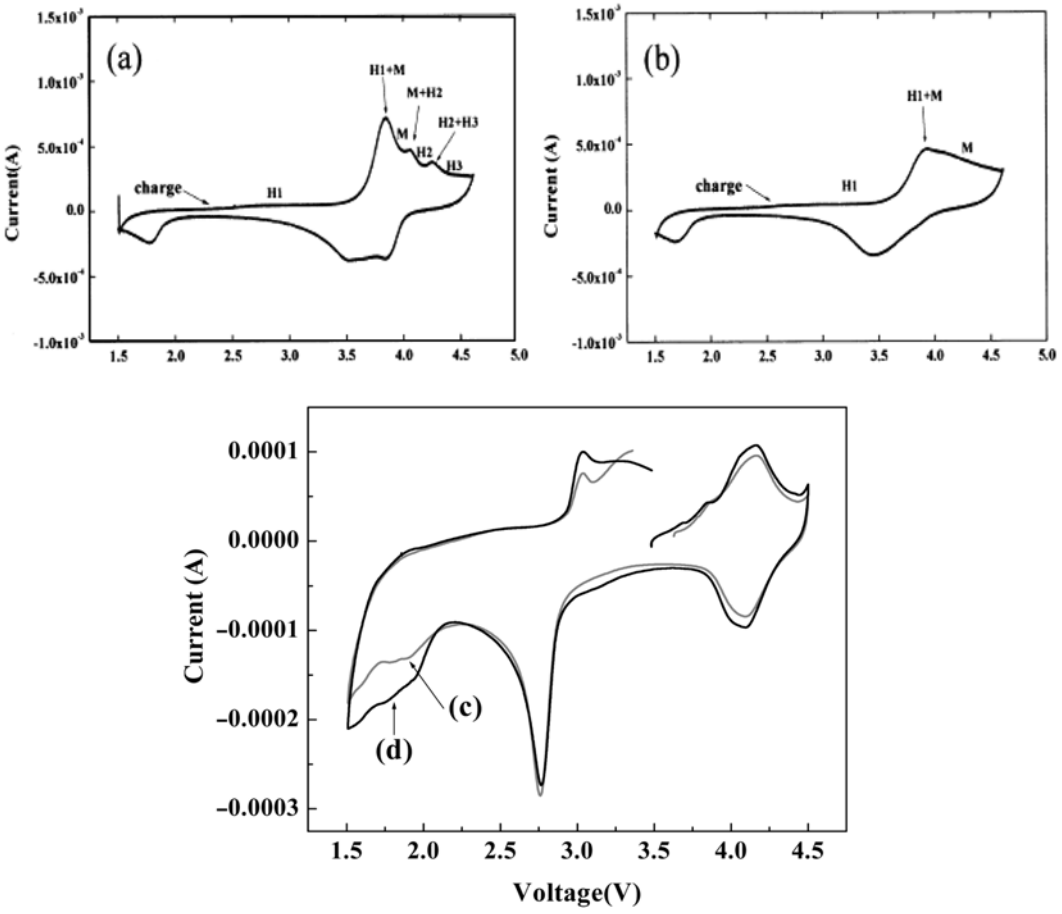

Fig. 7. Cyclic voltammogram of (a) Li/$Li_{1-x}FeO_2$-Li_xMnO_2 (Fe+Ni+Mn)=0.8) and (b) Li/$Li_{1-x}Fe_{0.8}Ni_{0.2}O_2$-$Li_xMnO_2$ (Mn/(Fe+Ni+Mn)=0.8) cells. The scan rate was 0.2 mV/s between 4.5 and 1.5 V at 25 °C.

monly occurred below 2.0 V; however, the original Li/$Li_{1-x}FeO_2$-Li_xMnO_2 cell suffered from much serious structural change in this voltage region.

Many research groups have reported the effects of substituted transition metal ions in the original structure by theoretical and electrochemical analyses [21-24]. We also found and reported that the Li/$LiNiO_{1.9}S_{0.1}$ cell suppressed serious phase changes of the Li/$LiNiO_2$ system during the charge/discharge process by CV analysis, which greatly improved the cell stability of the Li/$LiNiO_2$. Sulfur doping induced a remarkable improved cycle retention rate of the Li/$LiNiO_{2-y}S_y$ cell which is superior to that of $LiNiO_2$. However, the initial capacity of the sulfur-doped cell decreases with the increases of sulfur content doped in the material. Based on the previous study, a CV measurement was conducted on the $Li_{1-x}FeO_2$-Li_xMnO_2 and $Li_{1-x}Fe_{0.8}Ni_{0.2}O_2$-$Li_xMnO_2$ materials at 0.2 mV/s scan rate between the voltage limits of 1.5-4.5 V. The counter and reference electrodes were prepared by pressing lithium foil onto stainless steel gauze. Fig. 7 shows the cyclic voltammogram of the Li/$Li_{1-x}FeO_2$-Li_xMnO_2 and Li/$Li_{1-x}Fe_{0.8}Ni_{0.2}O_2$-$Li_xMnO_2$ cells. The cyclic voltammograms of the two systems are very similar except the voltage curve shape between 2.0 and 1.5 V. It could be expected that the difference of shape in this voltage region could be a main clue to explain the unique cycle behavior of the Li/$Li_{1-x}Fe_{0.8}Ni_{0.2}O_2$-$Li_xMnO_2$ system, which shows a high initial discharge capacity and a good cycleability simultaneously. Furthermore, the CV curve in this voltage region shows well the effect of nickel ion in the Li/$Li_{1-x}Fe_{0.8}Ni_{0.2}O_2$-$Li_xMnO_2$ cell, which suppressed the structural change of the original $Li_{1-x}FeO_2$-Li_xMnO_2 cell. The reduction peak of Li/$Li_{1-x}FeO_2$-Li_xMnO_2 cell happened rapidly changing between 2.0 and 1.5 V and this indication happened more seriously below 1.7 V. However, the Li/$Li_{1-x}Fe_{0.8}Ni_{0.2}O_2$-$Li_xMnO_2$ system showed a broad shape and no abrupt change between the 2.0 and 1.5 V region. It also showed a big reduction peak in this voltage region, which means the occurrence of an active electrochemical reaction in the Li/$Li_{1-x}Fe_{0.8}Ni_{0.2}O_2$-$Li_xMnO_2$ cell. This indication explains well why the Li/$Li_{1-x}Fe_{0.8}Ni_{0.2}O_2$-$Li_xMnO_2$ cell showed a good cycle retention rate during cycling, though it exhibited an increased initial discharge capacity compared with the original $Li_{1-x}FeO_2$-Li_xMnO_2 cell. From the above results, we strongly suggest that the structural change between 2.0 and 1.5 V has a very important key phenomenon to reveal the cycle mechanism of the original and Ni-substituted Li/$Li_{1-x}FeO_2$-Li_xMnO_2 systems. Also, *ex-situ* XPS analysis was conducted to investigate the change of valence state for various metal ions for the two systems in the same voltage region.

Table 2 shows the results of *ex-situ* XPS analyses for Li/$Li_{1-x}FeO_2$-Li_xMnO_2 and Li/$Li_{1-x}Fe_{0.8}Ni_{0.2}O_2$-$Li_xMnO_2$ cells after the first charge/discharge process. Each cell was left in a glove box for 2 days to reach equilibrium after being tested from 1.5 V to 4.5 V. In the charge

Table 2. The results of *ex-situ* XPS analysis for $Li/Li_{1-x}FeO_2$-Li_xMnO_2 (Mn/Fe+Ni+Mn=80%) and $Li/Li_{1-x}Fe_{0.8}Ni_{0.2}O_2$-$Li_xMnO_2$ (Mn/Fe+Ni+Mn=80%) cells during charge/discharge process

	$Li/Li_{1-x}FeO_2$-Li_xMnO_2	$Li/Li_{1-x}FeO_2$-Li_xMnO_2
Fe	+3	+3
Ni	+2→+2, +3→+2	
Mn	+4→+3, +4→+4	+4→+3, +4→+4

process, there is the oxidation reaction of Mn^{3+}/Mn^{4+}, from which was supposed a very small amount of Mn^{3+} remained in the raw material, although the XPS results of the two raw materials showed commonly 4+. The XPS results of the two cells clearly showed the movement of Mn ions from 3+ to 3+, 4+ (mixed state), and then, it was completely transformed into 4+ (Mn $2p_{3/2}$=642.75 eV) at the end of the charge process (4.5 V). The nickel ion in the $Li_{1-x}Fe_{0.8}Ni_{0.2}O_2$-$Li_xMnO_2$ keeps a valence state of 2+ in the raw material. However, the nickel ion in the $Li/Li_{1-x}Fe_{0.8}Ni_{0.2}O_2$-$Li_xMnO_2$ cell changed from 2+ (Ni $2p_{3/2}$=854.18 eV) to 3+ (Ni $2p_{3/2}$=855.65 eV) and this cell maintained a mixed state of 2+ and 3+ at the end of charge state maintaining the larger amount of Ni^{3+} ions.

On the other hand, in the discharge process, the valence state of Mn ions gradually changed from 4+ to 3+ and mixed ions states of Mn^{4+} and Mn^{3+} stayed until the 2.1 V region. However, the valence state of Mn ions rapidly converted into the 4+ between 2.0 and 1.5 V region, of which a serious structural change occurred in the CV and *ex-situ* XRD diagram. Also, the mixed state of 2+ and 3+ of Ni ions in the $Li/Li_{1-x}Fe_{0.8}Ni_{0.2}O_2$-$Li_xMnO_2$ cell also started to be moved at 2+ together with starting the discharge process. Fig. 8 shows the *ex-situ* XPS spectra of Ni $2p_{3/2}$ of various $Li_{1-x}Fe_{0.8}Ni_{0.2}O_2$-$Li_xMnO_2$ electrodes during the first discharge process. It stayed two mixed states with 2+ and 3+ until 2.4 V region and gradually reduced the amount of Ni^{3+} ions between 2.0 and 1.5 V region. The values of peak BE are 855.72 eV (Ni^{3+}) at 3.6 V and 855.46 eV for (Ni^{2+}) at 1.5 V in the discharge process. From the *ex situ*-XPS result, we concluded that original and nickel substituted $Li/Li_{1-x}FeO_2$-Li_xMnO_2 cells showed commonly large discharge capacities, due to the redox couple of Mn^{3+}/Mn^{4+} during charge/discharge process. Furthermore, the $Li/Li_{1-x}Fe_{0.8}Ni_{0.2}O_2$-$Li_xMnO_2$ cell exhibited better cycle properties than the original $Li/Li_{1-x}FeO_2$-Li_xMnO_2, owing to the oxidation/reduction reaction of Ni^{2+}/Ni^{3+} between the 2.0 and 1.5 V region.

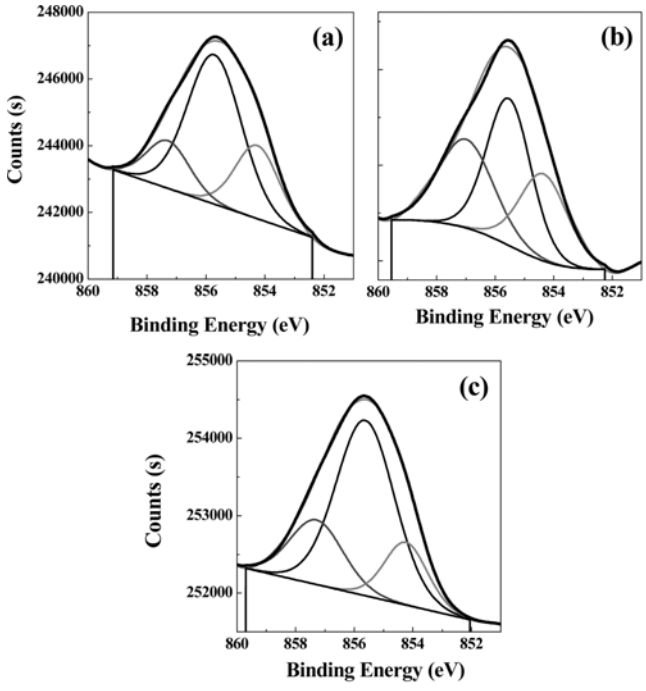

Fig. 8. *Ex-situ* XPS spectra of Ni$2p_{3/2}$ of various $Li_{1-x}Fe_{0.8}Ni_{0.2}O_2$-$Li_xMnO_2$ (Mn/(Fe+Ni+Mn)=0.8) electrodes during the first discharge process. (a) 3.6 V, (b) 1.9 V, and (c) 1.5 V.

CONCLUSION

$Li_{1-x}Fe_{0.8}Ni_{0.2}O_2$-$Li_xMnO_2$ (Mn/(Fe+Ni+Mn)=0.8) material was synthesized at 350 °C in an air by conventional solid-state method. It was composed of many large particles of about 500-600 nm and small particles of about 100-200 nm, which were distributed among the larger particles. The $Li/Li_{1-x}Fe_{0.8}Ni_{0.2}O_2$-$Li_xMnO_2$ cell showed a high initial discharge capacity above 192 mAh/g, which was higher than that of the parent $Li/Li_{1-x}FeO_2$-Li_xMnO_2 (186 mAh/g). This cell also exhibited an excellent cycle retention rate (96%) after 45 cycles. We concluded that the increased initial discharge capacity of $Li/Li_{1-x}Fe_{0.8}Ni_{0.2}O_2$-$Li_xMnO_2$ cell resulted from the redox reaction of Ni^{2+}/Ni^{3+} between 2.0 and 1.5 V region.

ACKNOWLEDGMENT

This work was supported by the Korea Electrical Engineering & Science Research Institute by Korea Government (2007).

REFERENCES

1. K. Mizushima, P. C. Jones, P. J. Wiseman and J. B. Goodenough, *Mater. Res. Bull.*, **15**, 783 (1980).
2. E. Rossen, J. N. Reimers and J. R. Dahn, *Solid State Ionics*, **62**, 53 (1993).
3. T. Ohzuku, A. Ueda, M. Nagayama, Y. Iwakoshi and H. Komori, *Electrochim. Acta*, **38**, 1159 (1993).
4. D. H. Jang, Y. J. Shin and S. M. Oh, *J. Electrochem. Soc.*, **143**, 2204 (1996).
5. Y. Xia, Y. Zhou and M. Yoshio, *J. Electrochem. Soc.*, **144**, 2593 (1997).
6. Y. Xia and M. Yoshio, *J. Power Sources*, **57**, 125 (1995).
7. R. Kanno, T. Shirane, Y. Kawamoto, Y. Takeda, M. Takano, M. Ohashi and Y. Yamaguchi, *J. Electrochem. Soc.*, **143**, 2435 (1996).
8. T. Shirane, R. Kanno, Y. Kawamoto, Y. Takeda, M. Takano, T. Kamiyama and F. Izumi, *Solid State Ionics*, **79**, 227 (1995).
9. M. Tabuchi, K. Ado, H. Sakaebe, C. Masquelier, H. Kageyama and O. Nakamura, *Solid State Ionics*, **79**, 220 (1995).
10. M. Tabuchi, C. Masquelier, T. Takeuchi, K. Ado, I. Matsubara, T. Shirane, R. Kanno, S. Tsutsui, S. Nasu, H. Sakaebe and O. Nakamura, *Solid State Ionics*, **90**, 129 (1996).
11. K. Ado, M. Tabuchi, H. Kobayashi, H. Kageyama, O. Nakamura, Y. Inaba, R. Kanno, M. Takagi and Y. Takeda, *J. Electrochem. Soc.*, **144**, L177 (1997).

12. M. Tabuchi, K. Ado, H. Kobayashi, I. Matsubara, H. Kageyama, M. Wakita, S. Tsutsui, S. Nasu, Y. Takeda, C. Masqulier, A. Hirano and R. Kanno, *J. Solid State Chem.*, **141**, 554 (1998).
13. M. Tabuchi, S. Tsutsui, C. Masquelier, R. Kanno, K. Ado, I. Matsubara, S. Nasu and H. Kageyama, *J. Solid State Chem.*, **140**, 159 (1998).
14. Y. Sakurai, H. Arai, S. Okada and J. Yamaki, *J. Power Sources*, **68**, 711 (1997).
15. Y. Sakurai, H. Arai and J. Yamaki, *Solid State Ionics*, **113-115**, 29 (1998).
16. Y. S. Lee, S. Sato, M. Tabuchi, C. S. Yoon, Y. K. Sun, K. Kobayakawa and Y. Sato, *Electrochem. Comm.*, **5**, 549 (2003).
17. Y. S. Lee, S. Sato, Y. K. Sun, K. Kobayakawa and Y. Sato, *Electrochem. Comm.*, **5**, 359 (2003).
18. Y. S. Lee, C. S. Yoon, Y. K. Sun, K. Kobayakawa and Y. Sato, *Electrochem. Comm.*, **4**, 727 (2002).
19. Y. S. Lee and M. Yoshio, *Electrochem. Solid-State Lett.*, **4**(10), A166 (2001).
20. Y. S. Lee, C. S. Yoon, Y. K. Sun and M. Yoshio, *Electrochem. Solid-State Lett.*, **5**(1), A1 (2002).
21. S. G. Youn, I. H. Lee, C. S. Yoon, C. K. Kim, Y. K. Sun, Y. S. Lee and M. Yoshio, *J. Power Sources*, **108**(1-2), 97 (2002).
22. Y. Ito, Y. Idemoto, Y. Tsunoda and N. Koura, *J. Power Sources*, **119-121**, 733 (2003).
23. H. Ikuta, K. Takanaka and M. Wakihara, *Electrochim. Acta*, **414**(2), 227 (2004).
24. S. H. Park, K. S. Park, K. S. Nahm, Y. K. Sun, Y. S. Lee and M. Yoshio, *Electrochim. Acta*, **47**, 1721 (2002).